The electronic states of pyridine-N-oxide studied by VUV photoabsorption and ab initio configuration interaction computations

The electronic states of pyridine-N-oxide studied by VUV photoabsorption and ab initio configuration interaction computations

Michael H. Palmer, Søren Vrønning Hoffmann, Nykola C. Jones, Elliott R. Smith, and Dennis L. Lichtenberger

Citation: The Journal of Chemical Physics **138**, 214317 (2013); doi: 10.1063/1.4807841
View online: http://dx.doi.org/10.1063/1.4807841
View Table of Contents: http://scitation.aip.org/content/aip/journal/jcp/138/21?ver=pdfcov
Published by the AIP Publishing

The electronic states of pyridine-N-oxide studied by VUV photoabsorption and *ab initio* configuration interaction computations

Michael H. Palmer,[1,a)] Søren Vrønning Hoffmann,[2,a)] Nykola C. Jones,[2,a)] Elliott R. Smith,[3] and Dennis L. Lichtenberger[3,a)]

[1]*School of Chemistry, University of Edinburgh, West Mains Road, Edinburgh EH9 3JJ, Scotland, United Kingdom*
[2]*ISA, Department of Physics and Astronomy, Aarhus University, Ny Munkegade 120, DK-8000 Aarhus C, Denmark*
[3]*Department of Chemistry and Biochemistry, The University of Arizona, Tucson, Arizona 85721, USA*

(Received 17 March 2013; accepted 13 May 2013; published online 7 June 2013)

The first vacuum-ultraviolet absorption spectrum of pyridine-N-oxide has been obtained, and has led to the identification of nearly 30 Rydberg states. These states were identified by use of the vibrational envelope ("footprint") of the UV-photoelectron spectrum, and are based on the first to the third ionization energies (IE). The adiabatic IE order, central to the Rydberg state symmetry identification, is confirmed by multi-configuration SCF calculations as: $1^2B_1 < 1^2B_2 < 1^2A_2 < 2^2B_1$. Several excited valence state equilibrium structures were determined by multi-configuration SCF and coupled cluster procedures. Multi-reference multi-root CI was used to calculate both Rydberg and valence state vertical excitation energies and oscillator strengths, which were correlated with the experimental measurements. © *2013 AIP Publishing LLC*. [http://dx.doi.org/10.1063/1.4807841]

I. INTRODUCTION

Pyridine-N-oxide (**1** in Fig. 1, abbreviated to **PyNO**) is the simplest N-oxide of the azines, a class of fully conjugated heterocyclic compounds.[1–4] The importance of **PyNO** is demonstrated by the number of studies of its molecular structure, with several microwave (MW) substitution structures (having differing isotopic compositions),[5–8] electron diffraction (ED),[9] and x-ray diffraction[10] studies. The N-oxides are obtained by the oxidation of the corresponding azines such as pyridine (**2** in Fig. 1), but the properties of **1** and **2** (Fig. 1) are totally different; **1** readily undergoes electrophilic substitution at the 4-(γ)-position, whereas **2** is substituted only under extreme conditions at the 3- and 5-(β)-positions. The electron distribution of the ground state of **PyNO**, which has recently been reconsidered, is probably best represented by **1a.**[11] The frontier molecular orbitals of **PyNO** are shown in Fig. 2. Direct integration of the electron density[11] shows no increase of the electron density at the 4-(γ)-position in the ground state molecule so that the para-reactivity of **PyNO** with an electrophile[11] appears to be a polarization effect at the time of reaction, leading to canonical forms expressed by **1c**.

Previous spectroscopic studies of **PyNO** have been limited to the UV absorption[12–18] and the UV-photoelectron spectral (UPS) He I and He II regions.[19,20] The present paper extends the spectroscopic absorption range of **PyNO** into the vacuum ultraviolet (VUV) region up to 10.8 eV, where we have identified a number of Rydberg states. We have also calculated the equilibrium structures for several low-lying valence states, and determined a wider range of vertical excitation energies and oscillator strengths for both the valence and Rydberg states.

The vibrational "footprint" of the UPS occurs in Rydberg states,[21–23] since when an excited electron becomes distant from the nuclei, its potential becomes similar to that for ionization. Identification of the Rydberg states in the VUV spectrum of **PyNO** used the well-established procedure[24–27] of superimposing the UPS band profiles on the VUV spectrum. We have recently demonstrated the synergistic value of UPS and VUV absorption spectroscopy.[28,29]

The study of molecular Rydberg states occupies an important place in molecular spectroscopy,[21–23] and comprehensive accounts of their properties have been given for a variety of molecular species;[30–43] this remains an active area of research for both experimentalists and theoreticians. The energies of Rydberg states are given by term values[21–23] as follows:

$$Term\ value = IE - E_m = \frac{R}{(n-\delta)^2}, \qquad (1)$$

where IE is each adiabatic ionization energy (IE^A) and E_m is the mth Rydberg state energy level; R is the Rydberg constant, while n is the principal quantum number, and δ is the quantum defect. The lowest Rydberg states have $n = 3$; the values of δ for s-, p-, d-, and f-states are progressively smaller with values $\delta \geq 0.75$, 0.4–0.6, 0.1–0.2, and 0.0–0.1, respectively.[21–29]

II. EXPERIMENTAL AND COMPUTATIONAL PROCEDURES

A. Experimental VUV and UPS procedures

PyNO (CAS Registry No. 694-59-7, Sigma-Aldrich) is hygroscopic and was purified by repeated distillation and

a)Authors to whom correspondence should be addressed. Electronic addresses: m.h.palmer@ed.ac.uk; vronning@phys.au.dk; nykj@phys.au.dk; and dlichten@email.arizona.edu

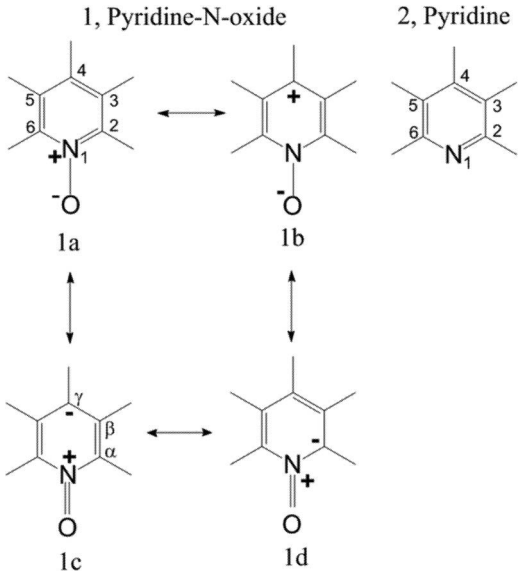

FIG. 1. Pyridine-N-oxide (**1**) and pyridine (**2**) including canonical (resonance) structures.

stored in an inert atmosphere. The VUV spectrum (Fig. 3, and discussed below) was recorded using the UV1 beam line on the ASTRID storage ring at Aarhus University, Denmark; the procedure has been described previously.[28,29] The gas cell and sample container, held at 55 °C during the measurements,

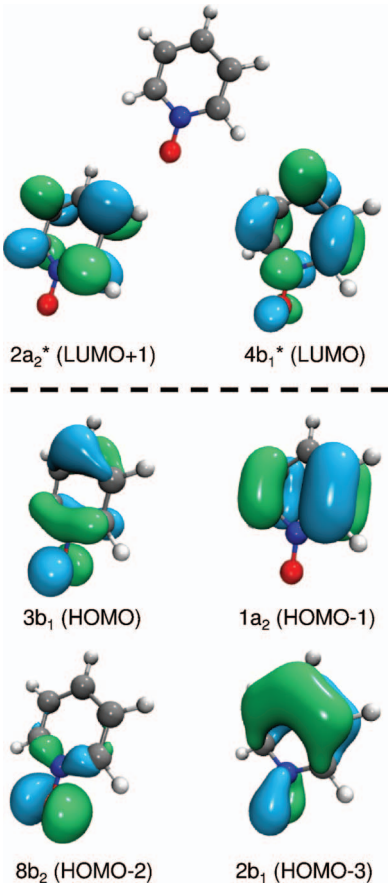

FIG. 2. The dominant set of MOs in the low-lying excited and ionized states (shown at HF/cc-pVTZ level in Aufbau sequence order).

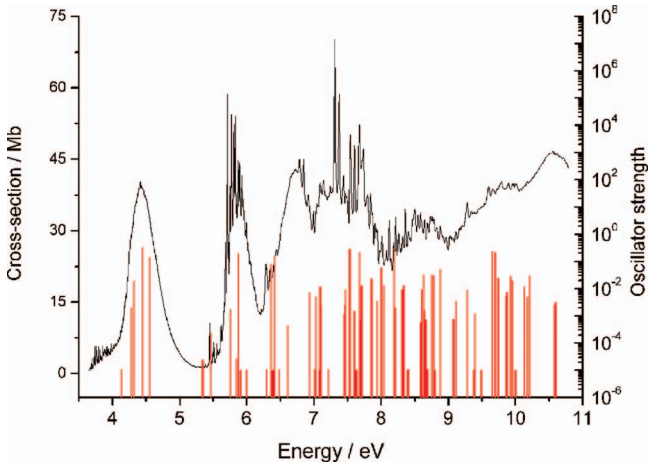

FIG. 3. Calculated valence states superimposed on the measured UV+VUV spectrum; $^1A_2$ states have been given an arbitrary f(r) = 1×10^{-5} in order to indicate their positions.

gave a sample vapor pressure of 0.02 Torr. The absorption cross-section was corrected for water absorption using a high resolution water spectrum.[44]

Previously available UPS studies[19] for **PyNO** report several vibrational intervals, but the published figures are so heavily reduced in size that they are unsuitable for the vibrational footprint to be superimposed on the VUV spectral regions, which are frequently complex. Thus we have remeasured the four lowest bands of the UPS spectrum as discussed further below; the vibrational intervals reproduce previous values.[19] Further details of the UPS spectrum and its interpretation are given in the supplementary material.[45]

B. Computational methods

The *ab initio* calculations were performed with modules from GAMESS-UK,[46] and MOLPRO[47] suites of programs. High levels of multi-reference configuration interaction were essential to obtain excitation energies close to experiment.

1. MCSCF procedures

Calculation of the adiabatic singlet excited and ionic state structures and energies used state-averaged (SA) MCSCF techniques with MOLPRO. The structural results are described in the supplementary material[45] and were performed with the cc-pVTZ basis set.[48] Since many of the low energy **PyNO** excitations are $\pi\pi^*$ states, all π-electrons were included in the MCSCF variable occupancy set. The final choice was 12 electrons distributed over 14 valence MOs (14MO12e); electrons from the doubly occupied SCF orbitals $13a_1$, $1b_1$, $2b_1$, $3b_1$, $8b_2$, and $1a_2$ (DOMOs); these were distributed among 3, 5, 3, and 3 MOs of a_1, b_1, b_2, and a_2 symmetry, respectively.

Throughout this study, it was found that the excited states were dominated by the MOs shown in Fig. 2. In a generalized description of the overall spatial wavefunction, the two highest occupied orbitals ($3b_1$ and $1a_2$) have two nodal surfaces separating four orbital lobes in the pyridine portion of the molecule, and thereby are classified as primarily *d*-type

orbitals in a spherical model. The next two occupied orbitals in Fig. 2 ($8b_2$ and $2b_1$) also have two nodal surfaces separating four orbital lobes including the NO portion of the molecule and are likewise classified as *d*-type orbitals. The lowest unoccupied orbitals ($2a_2^*$ and $4b_1^*$) have three nodal surfaces separating eight orbitals lobes in the pyridine portion of the molecule and thereby are classified as *f*-type orbitals. In the approximation of a spherical model, electronic excitation from these valence occupied orbitals to the lowest unoccupied orbitals is a *d*-to-*f* type allowed transition in each case. The close analogy with the MOs of benzene ($1e_{1g}$ and $1e_{2u}^*$), and especially chlorobenzene is important; similar relationships have been noted from the analysis of excited state vibrational structure.[14–18]

2. Multi-reference multi-root doubles and singles CI method (MRD-CI)

The most successful method for calculating the vertical excitation energies to correlate with the experimental VUV envelope used the MRD-CI.[49–51] This procedure has recently been reviewed,[38] and is implemented in GAMESS-UK.[46] The valence excited states were obtained using the aug-cc-pVTZ basis sets.[52] However, the lowest exponents of *s*- and *p*-type in aug-cc-pVTZ basis sets interact with the (even lower) exponents of the Rydberg state study to cause near zero eigenvalues of the overlap matrix; this results in linear dependence. Thus the Rydberg state studies were built on a TZVP (triple-zeta valence with polarization) basis[53] augmented with *s-, p-, and d*-Rydberg state exponents at the centre of mass;[28,29,54] the smaller set contained [4*s*3*p*3*d*] (TZVPR basis set), while the necessity of seeking solutions for the Rydberg state members above $n = 5$ (Eq. (1)), required a [6*s*6*p*6*d*] set. The theoretical band intensities were evaluated from the calculated oscillator strengths $f(r)$ using the CI wave functions within the MRD-CI[38,49–51] modules; the wide difference in oscillator strength enables differentiation between valence and Rydberg states, since typical values for $f(r)$ are 10^{-1}–10^{-2} and 10^{-2}–10^{-6}, respectively.[38] The character of the vertical singlet states is also shown by the second moments (SM) of the charge distribution ($\langle x^2\rangle$, $\langle y^2\rangle$, and $\langle z^2\rangle$). In the present study, valence states have SM values in the range from −30 to −50 a.u.^{2}; Rydberg states give numerically much larger values up to −550 a.u.^{2} depending on the principal quantum number, and a more directional character (X, Y, Z, etc.). Further details of the theoretical methods employed, including basis sets, are given in the supplementary material.[45]

3. UCCSD(T) and UB3LYP procedures

These used unrestricted (U) variations of the coupled cluster procedure CCSD(T), and B3LYP variety of density functional methods (DFT), and were limited to the ionic state (open shell) calculations. As with the MCSCF structural results (as described in the supplementary material[45]) they were performed with the cc-pVTZ basis set[48] within the MOLPRO suite.[47]

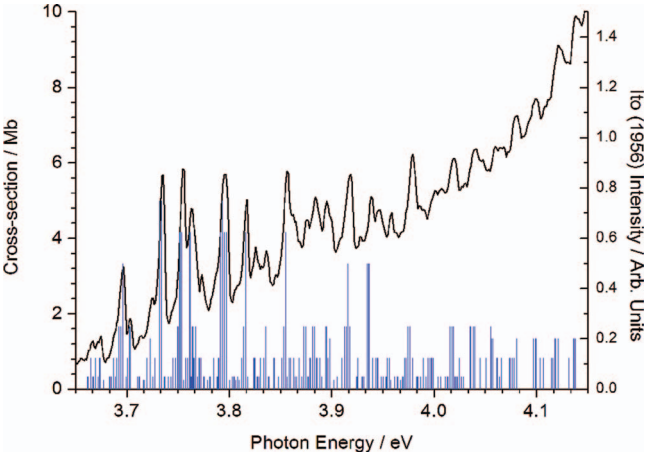

FIG. 4. Superposition of the present UV onset for **PyNO**, together with the stick diagram based on data extracted by Ito and Mizushima[12] from their photographic image.

III. THE UV + VUV PHOTOABSORPTION SPECTRUM OF PyNO

The UV+VUV region from 3.6 to 10.8 eV ("wide scan") is shown in Fig. 3. For simplicity and convenience, our calculated valence states for vertical excitation, which are discussed below, are shown superimposed on the spectrum; the $^1A_2$ states have been given an arbitrary $f(r) = 1 \times 10^{-5}$ in order to indicate their positions.

The absorption spectrum onset in the near UV region (27 400–33 400 cm^{-1}) was previously measured by Ito and Mizushima[12] using a quartz spectrograph; this enabled them to identify nearly 250 bands in this range. Subsequently, Bist and Parihar[16,17] performed an analysis of the vibrational structure and identified all 30 fundamentals. Our long wavelength spectral limit is 29 214 cm^{-1} (3.622 eV); hence the 0–0 band (29 299 cm^{-1}, 3.633 eV)[13,16] of the lowest UV transition for **PyNO** was not observed in our study. A comparison of these previously reported electronic transition results with our low energy range (Fig. 4) confirms the main peak positions.

IV. COMPUTATIONAL RESULTS

A. The ground and cationic structures

The final confirmation of the order of the first 5 ionic states as $1^2B_1 < 1^2B_2 < 1^2A_2 < 2^2B_1 < 1^2A_1$ is discussed below. In our hands, it is only practicable to use CCSD(T) for first states of each symmetry; in order to include both the 1^2B_1 and 2^2B_1 states, we used SA-MCSCF, as well. For the calculated structure of the $\tilde{X}\ ^1A_1$ state, the average differences in bond lengths and angles from the MW substitution structure[5–8] are 0.0014 Å and 0.30°, respectively, while the internal ring angles follow the MW sequence of magnitudes: $C_{2,6} > C_{3,5} > N_1 > C_4$. Since these ground state structural differences from the experimental MW structure are very small, this leads to confidence that the excited and ionic state structures are realistic. Several excited state structures, determined by using the SA-MCSCF method, show significant structural

TABLE I. Adiabatic excitation energies determined by using MCSCF method, with selected low-lying singlet valence state vertical excitation energies (eV) calculated by the MRD-CI method. Also shown are oscillator strengths, and second moments (a.u.).

Adiabatic MCSCF [a]			Vertical MRD-CI [b,c,d]				
Energy (eV)	Energy (eV)	$10^6 f(r)$	Symmetry	Leading term	$\langle x^2 \rangle$	$\langle y^2 \rangle$	$\langle z^2 \rangle$
0.00	0.00		X^1A_1	Ground state	−33.1	−25.1	−36.2
3.65	4.32	181 58	1^1B_2	$3b_1 2a_2^*$	−47.1	−28.7	−32.7
4.33	4.13	0	1^1A_2	$8b_2 4b_1^*$	−38.1	−29.4	−30.9
4.61	4.45	317 642	1^1A_1	$3b_1 4b_1^*$	−37.4	−29.4	−34.4
5.68	5.34	24	1^1B_1	$8b_2 2a_2^*$	−40.8	−35.1	−29.8
6.02	5.46	236	2^1B_1	$3b_1 17a_1^*$	−49.7	−51.2	−55.9
6.37	6.37	73 562	2^1A_1	$3b_1 5b_1^*$	−61.4	−32.6	−39.8
6.39	6.39	0	2^1A_2	$1a_2 13a_1^*$	−48.8	−41.4	−70.0
6.41	6.41	145 026	3^1A_1	$2b_1 4b_1^*$	−39.4	−34.4	−38.6
6.52	7.75	176 610	3^1B_2	$2b_1 2a_2^*$	−55.1	−35.1	−42.2
[e]	4.28	1902	3^1B_1	$3b_1 13a_1^*$	−52.2	−39.9	−85.8
[e]	4.56	139 613	4^1A_1	$1a_2 2a_2^*$	−40.2	−31.3	−39.6
[e]	5.88	182 636	2^1B_2	$3b_1 3a_2^*$	−46.6	−37.6	−34.7
[e]	7.53	278 191	4^1B_2	$1a_2 4b_1^*$	−60.6	−37.4	−36.7
[e]	6.00	0	3^1A_2	$3b_1 9b_2^*$	−46.0	−79.5	−43.9

[a]Excitation energies are relative to the $\tilde{X}\ ^1A_1$ ground state CI energy −321.77219 a.u.
[b]Basis set total Cartesian and harmonic basis functions 303 and 282, respectively.
[c]Orbital occupancy 1-13a_1 1-3b_1 1-8b_2 1a_2; active MOs 8–156.
[d]Excitation energies are relative to the $\tilde{X}\ ^1A_1$ ground state CI energy −322.23600 a.u.
[e]We were unable to obtain a convergent MCSCF result for these higher states having these dominant configurations.

differences from the ground state and are shown in the supplementary material.[45]

B. The calculated singlet excited valence states

The lowest lying excited states (Table I) are sequenced by the MCSCF equilibrium energies, which are regarded as the most reliable excited singlet state energies. In some cases, there are significant differences between the adiabatic (MCSCF) and vertical (MRD-CI) excitation energies. Some significant structural changes occur on excitation and the N–O bond is the most susceptible to change with electronic state, as expected from the dipolar nature of the group. Unusually, the pair of low-lying $^1A_1$ $\pi\pi^*$-states ($3b_1 4b_1^*$, and $1a_2 2a_2^*$) occur as almost entirely separate solutions, rather than as linear combinations; these are separated by 0.11 eV (vertical) and 2.82 eV (adiabatic). The pair of valence $^1B_1$ states ($3b_1 13a_1^*$) and ($8b_2 2a_2^*$), occur at unexpectedly low energy in the vertical study where they are separated by ∼1 eV, but only by 0.34 eV in the MCSCF study; this is almost certainly a result of the simultaneous state average of 4 MCSCF states, leading to the mixing of the states of same symmetry with widely differing relaxation energies. These lead to more dramatic effects than are possible in the vertical study using the ground state geometry.

However, although the vertical excitation energies are less reliable, they are accessible for many more excited states, and their intensities give a guide to the positions of prominent peaks in the VUV spectrum. Vertical excitation energies for valence and Rydberg states are shown in Tables I and II, respectively, and further results are given in the supplementary material.[45] The present groupings of calculated valence states are consistent with the observed high intensity peaks of the VUV spectrum (Fig. 3). A major spectroscopic feature apparent in Fig. 3 is the absence of absorption between 5 and 5.5 eV. This gap is reproduced by the MRD-CI calculations, but several other widely used vertical excitation methods including TD-HF, TD-DFT, and EOM-CCSD were found to be unsatisfactory for this region, and these other methods were abandoned for this reason.

All the most intense calculated bands (Table I) are of $^1B_2$ and $^1A_1$ symmetry, suggesting difficulty in experimental location of the $^1B_1$ (and optically forbidden $^1A_2$) states. The present calculations support the accepted view[16,17] that the onset of the broad UV band between 4 and 5 eV is the $^1B_2$ state. The broad band between 4 and 5 eV probably contains several electronic states. Using the calculated excitation energies shown in Table I, the series of singlet states, 1^1A_2, 1^1A_1, 1^1B_1, and 2^1B_1 states are thought to occur here, probably accompanied by related triplet states; we are unable to reliably determine the sequence of states by symmetry. In some instances, the vertical excitation energies are apparently lower than the MCSCF ones. These anomalies are artefacts since the MRD-CI method allows much higher excitations to be included in the CI (up to 8 open shells) than are possible with the MCSCF. Also, the MCSCF and MRD-CI results occurring on the same line in Table I have similar leading terms in their respective CI expansions, but significant other differences occur in some cases.

C. The calculated Rydberg states

The Rydberg and valence states were calculated together, and here we used the TZVPR basis set as described in

TABLE II. Calculated Rydberg states for pyridine-N-oxide correlated with experimentally identified states in Table IV. These MRD-CI results show vertical excitation energies (eV), oscillator strengths, and second moments (a.u.).[a,b,c] Further vertical excited states are shown in the supplementary material.[45]

Energy (eV)	$10^6 f(r)$	Symmetry	Leading term	$\langle x^2 \rangle$	$\langle y^2 \rangle$	$\langle z^2 \rangle$
5.50	3106	1^1B_1	$3b_1S$	− 55.3	− 52.0	− 80.0
6.37	531	2^1B_1	$3b_1Z$	− 68.9	− 86.2	− 78.6
6.49	1725	3^1B_1	$3b_1XX\text{-}YY$	− 196.0	− 141.8	− 73.2
6.68	81	4^1B_1	$3b_1S$	− 96.2	− 98.1	− 133.1
6.91	6977	1^1A_1	$3b_1XZ$	− 214.0	− 81.4	− 175.7
7.05	2499	5^1B_1	$3b_1Z$	− 114.6	− 120.6	− 140.1
7.06	3672	6^1B_1	$3b_1XX\text{-}YY$	− 184.3	− 127.0	− 79.6
7.18	2205	1^1B_2	$8b_2Z$	− 68.8	− 77.6	− 74.5
7.29	8304	2^1B_2	$3b_1XY$	− 195.3	− 184.8	− 78.8
7.62	1659	7^1B_1	$3b_1XX\text{-}YY$	− 226.5	− 177.3	− 84.5
7.67	975	8^1B_1	$3b_1Z$	− 147.4	− 201.6	− 282.9
7.68	61	3^1B_2	$8b_2Z$	− 110.6	− 116.0	− 134.7
8.06	4	4^1B_2	$8b_2S$	− 519.9	− 513.8	− 501.4
8.14	4572	5^1B_2	$3b_1XY$	− 235.4	− 225.1	− 91.5
8.26	125	6^1B_2	$8b_2ZZ\text{-}RR$	− 157.8	− 150.3	− 384.6
8.52	168	7^1B_2	$8b_2Z$	− 155.3	− 215.2	− 285.2
8.96	459	2^1A_1	$1a_2XY$	− 189.8	− 176.2	− 83.7
9.71	2078	3^1A_1	$1a_2XY$	− 201.6	− 187.9	− 87.7

[a]Basis set total Cartesian and harmonic basis functions 303 and 282, respectively.
[b]Orbital occupancy 1-13a_1 1-3b_1 1-8b_2 1a_2; active MOs 8−159.
[c]Excitation energies are relative to the $\tilde{X}\ ^1A_1$ ground state CI energy −322.29852 a.u.

Sec. II B. The low-lying valence states show very similar energies and oscillator strengths to those recorded in the valence state calculations (Table I), and are omitted from the list of Rydberg states (shown in the supplementary material). Rydberg states are identified by both the contributing MOs, and the second moments of the charge distribution (cf. Sec. II B), where typical values are listed in Table II. Rydberg states selected for correlation with experiment are discussed in Secs. VI C and VI D below. The calculated oscillator strengths of the valence and Rydberg states (Tables I and II) suggest that most experimental Rydberg states excitations will have low calculated intensity, in contrast to the valence states.

Pairs of Rydberg states with a common upper state have an excitation energy difference which is close to the difference between the ionization energies of their lower states. The ionization energy differences between the pairs of states ($^2B_1$ and $^2B_2$) and ($^2B_2$ and $^2A_2$) are 0.95 and 1.00 eV, respectively. A correlation of 15 Rydberg state excitation energies involving MOs $3b_1$ and $8b_2$ into the first shell ($n = 3$) with X, Y, Z, XY, XZ, and YZ upper states, has a mean separation of 0.91 eV. The corresponding $8b_2$ and $1a_2$ excitations lead to a mean difference of 1.11 eV. In a similar way, the difference between the $3b_1$nS and $8b_2$nS series for pairs of values where n varies from 3 to 7 is 0.81 eV. Although an exact comparison with experiment cannot be expected since the Rydberg state energy can be distorted by nearby valence states, these results are close to the IE differences. Examples of calculated valence-Rydberg mixing (Table II) are the $3b_1XZ$ and $3b_1XY$ states, where the oscillator strengths ($f(r)$) are 0.007 and 0.008, respectively, which are relatively large for such states. The relatively large dimensions of the second moments of the charge distribution (XZ and XY, respectively) leave no doubt that these are Rydberg states.

V. UPS RESULTS

A. The low energy UPS spectral assignment for pyridine-N-oxide

The low energy UPS region is shown in Fig. 5. The vertical and adiabatic IE (IE^A) values are coincident for IE_1 to IE_3, but differ for IE_4. The adiabatic ionization energies used in Eq. (1) for the Rydberg state analyses described below, are 8.39, 9.18, 10.19, and 11.40 eV, with probable errors of ±0.005 eV. The individual data points in the UPS spectra are separated by 0.0012 eV, so that a group of four data points were deemed sufficient to justify the above estimate. Maier *et al.*[19] give the sequence of IE as 8.38 (2), 9.22(2), 10.18(2), and 11.59 (2)(IE^V) eV.

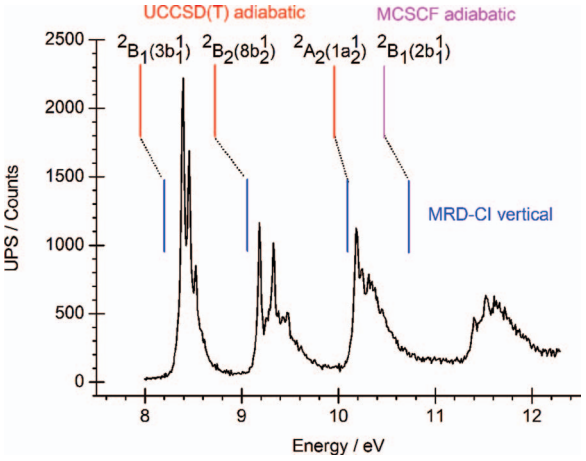

FIG. 5. The UPS low energy region used in the Rydberg state search, with the adiabatic (UCCSD(T) and MCSCF) and vertical (MRD-CI) assignments indicated.

TABLE III. Summary of the UPS experimental and theoretical results.

Ionization energy sequence	Experimental IE^A and IE^V (eV)	State	MO vacated in principal configuration	UCCSD(T) Adiabatic energy (eV)	MRD-CI Vertical energy (eV)	MRD-CI Density
IE_1	8.39 (A)	X	$3b_1$	7.98	8.18	0.892
IE_2	9.18 (A)	A	$8b_2$	8.73	9.08	0.915
IE_3	10.19 (A)	B	$1a_2$	9.99	10.12	0.896
IE_4	11.41(A), 11.52(V)	C	$2b_1$	10.46	10.74	0.849
IE_5	12.8(A), 13.02(V)	D	$13a_1$	12.90	13.40	0.900

It was only possible to obtain the lowest energy state of each symmetry by using the UCCSD(T) method (the most sophisticated method), but both the MCSCF and MRD-CI methods gave an equilibrium structure for the 2^2B_1 root (where MO $2b_1$ is vacated rather than a shake-up state). All three methods shown in Fig. 5 (and Table III) give the IE^A assignment as:, $1^2B_1 < 1^2B_2 < 1^2A_2 < 2^2B_1$ in accord with Maier *et al.*[19] who used variation of IE with ring-substitution pattern to generate their symmetry assignment. The CI methods calculate lower values for the adiabatic ionization energies than is observed in the experimental data. This arises from the much larger correlation energy determined by the CI for the open shell cation states; the number of contributing single plus double substitution configurations is markedly larger for open shell than related closed shell states. In effect, the CI is more effective at stabilizing the cations than the closed-shell neutral molecule. This is in contrast to calculations of ionization energies without CI which often overestimate the IE relative to experiment. Although not central to the present study, the IE_4 to IE_6 ionization processes correspond to ionization from the MOs $2b_1 < 7b_2 < 13a_1$. Further results of the study of the HeI and HeII regions of the UPS are given in the supplementary material.[45] The present UV+VUV energy range is from 3.6 to 10.8 eV (344–115 nm); Eq. (1) shows that the five lowest IE in the UPS of **PyNO** (as discussed below) will have 3*s* states (for $\delta = 0.9$, a typical value) with energies close to 5.3 ($3b_1$), 6.3 ($8b_2$), 7.1 ($1a_2$), 8.3 eV ($2b_1$), and 10.0 ($13a_1$). Higher IE will lead to Rydberg states beyond the current VUV energy range.

B. Rydberg state identification in the VUV spectrum

The overlay of the UPS and VUV spectra for identification of Rydberg states is well-established,[24–27,55,56] and relies on the vibrational patterns of both spectral processes being closely similar. The vibrational structural of IE_1 through to IE_3 was interpreted by Maier *et al.*[19] in terms of one, three, and one vibrational sequences, with frequencies $\tilde{X} = 520\ cm^{-1}$, $\tilde{A} = 1250, 810, 520\ cm^{-1}$, and $\tilde{B} = 480\ cm^{-1}$. Our results are consistent with these values, but we use the overall UPS structural form for comparison with the VUV spectrum. In that respect, the IE_1 ($\tilde{X}$) band shows that (Fig. 5) the full width at half height (FWHH) is ~0.030 eV, to be compared with the width of 0.006 eV for the VUV band in the 5–6 eV region (where the first Rydberg state is expected to occur); this difference is illustrated in Fig. 6. The present analysis of the VUV spectrum concentrates on IE_1 to IE_3 since IE_4 (MO vacated $2b_1$) is not resolved in sufficient detail for conclusive identification of Rydberg states; only a tentative example is given in the list shown in Table IV.

In the current analysis, overlay of the UPS and VUV spectra was performed progressively throughout the VUV range. The wide dynamic range of the VUV spectrum with differences in baseline slope under the Rydberg bands needs to be taken into account in this comparison; this is not unusual,[24,25] and the visual comparison was readily assisted by making the two baselines (VUV and UPS) parallel over the desired intervals, by removal of either a local sloping line or Gaussian peak from the VUV intensity. No variation in vibrational peak separation occurred in this pragmatic approach.

Although a variety of successful overlays occurred at higher energies, the lowest expected Rydberg state $3b_13S$ proved elusive; the value given in Table IV (and shown in Fig. 6) seems the most probable. The calculations indicate that this state has very low oscillator strength. Furthermore it also occurs in a spectral region where valence states of the same symmetry occur (Table II), including specifically the $3b_117a_1^*$ and $8b_22a_2^*$ states. Thus we believe that the VUV vibrational structure observed from 5.4 to 6.1 eV is valence in nature, which fortuitously has several vibrational intervals close to the single UPS band I frequency. Several groups of peaks in that region could be assigned to the UPS frequency, but it would be necessary to find a satisfactory interpretation

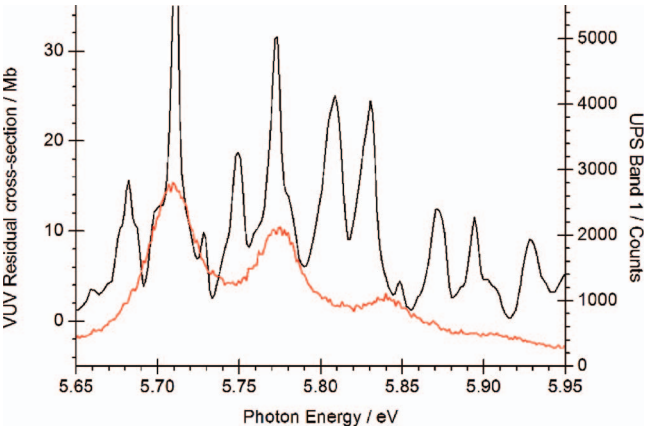

FIG. 6. The VUV spectrum (blue) with UPS superimposed (red). The Rydberg $3b_13S$ state is assigned to the broad structure near the base of the main bands. To increase the dynamic range of the structure, a broad underlying Gaussian peak has been subtracted from this energy range to assist the presentation of fine structure.

TABLE IV. Rydberg states observed in the VUV spectrum for Pyridine-N-oxide.

Observed Rydberg energy (eV)	IE-E based on IE of TABLE III	n	δ	Assignment	Calculated energy (eV)[a]
5.707	2.683	3	0.748	$3b_1 3S$	5.50
7.09	1.331	4	0.766	$3b_1 4S$	6.68
6.29,6.30	2.100	3	0.454[b]	$3b_1 3X$,$3b_1 3Z$	6.37
7.31	1.080	4	0.450[b]	$3b_1 4X$	7.05
7.73	0.660	5	0.459[b]	$3b_1 5X$	7.67
6.78	1.610	3	0.093[c]	$3b_1 3D$	6.49
6.85	1.540	3	0.037	$3b_1 3D'$	7.29
7.54	0.850	4	0.001[c]	$3b_1 4D$	7.06
7.84	0.550	5	0.026[c]	$3b_1 5D$	7.62
8.01	0.380	6	0.015[c]	$3b_1 6D$	8.14
8.36	0.826	5	0.941[d]	$8b_2 5S$	8.06
8.64	0.541	6	0.984[d]	$8b_2 6S$	
6.85	2.338	3	0.587[e]	$8b_2 3P$	7.18
7.94	1.244	4	0.692[e]	$8b_2 4P$	7.42
8.46	0.719	5	0.649[e]	$8b_2 5P$	8.20
7.03	2.156	3	0.488[f]	$8b_2 3P'$	7.18
8.12	1.067	4	0.429[f]	$8b_2 4P'$	7.68
8.55	0.638	5	0.381[f]	$8b_2 5P'$	8.52
8.19	1.001	4	0.313	$8b_2 4P''$	
8.26	0.928	4	0.170[g]	$8b_2 4D$	8.26
8.59	0.599	5	0.233[g]	$8b_2 5D$	
8.96	0.223	8	0.188[g]	$8b_2 8D$	
8.50	1.690	3	0.163[h]	$1a_2 3D$	8.58
9.28	0.910	4	0.133[h]	$1a_2 4D$	9.54
9.61	0.580	5	0.177[h]	$1a_2 5D$	9.95
9.79	0.400	6	0.146[h]	$1a_2 6D$	10.00
8.765	1.425	3	− 0.09	$1a_2 3D'$	
10.04	3.163	4	0.837	$2b_1 4S$	

[a]Least squares fit between the observed Rydberg state energies in column 1 (x) and the calculated ones in column 6 (y) with form: y = A + Bx has A = −0.54(48) and B = 1.06(6) where the standard deviations for the last digit are given. The median and maximum absolute errors are 0.26 and 0.52 eV.
[b]Series $\delta = 0.453(6)$, $IE_1 = 8.39(3)$.
[c]Series $\delta = 0.072(33)$, $IE_1 = 8.405(24)$.
[d]Series $\delta = 0.87$, $IE_2 = 9.15$.
[e]Series $\delta = 0.562(4)$, $IE_2 = 9.18(5)$.
[f]Series $\delta = 0.475(5)$, $IE_2 = 9.13(5)$.
[g]Series $\delta = 0.17(4)$, $IE_2 = 9.18(1)$.
[h]Series $\delta = 0.208(4)$, $IE_3 = 10.20(3)$.

of the difference in line width for this process alone, since it does not occur in Rydberg states elsewhere in this VUV spectrum. We believe that the broader line width of the UPS IE_1, which overlays (very precisely) several Rydberg states at higher energy, must be associated with broad features near the baseline of the VUV spectrum. Hence we arrive at the conclusion (Table IV) that the weak structure near 5.707 eV is the $3b_1 3S$ Rydberg state.

Systematic overlay of the UPS bands IE_1, IE_2, and IE_3 over sections of the VUV spectral envelope led to the identification of a number of Rydberg states summarized in Table IV. Most of these do not call for individual comment. Owing to congestion in the VUV spectrum at the highest energies above 10 eV, the process of identification of additional Rydberg states in the weak VUV bands is not yet possible.

Where several members of a Rydberg series have been identified in Table IV, these have been fitted to Eq. (1) in groups, allowing error determination by least squares fits. Single state solutions in Table IV, without error bars are direct use of Eq. (1). Where detailed analysis of a region leads to the interpretation in terms of two or more states of similar type, but different energies, these are listed in Table IV with primes, as in $3b_1 3D$ with $3b_1 3D'$, and $8b_2 4P'$ with $8b_2 4P''$. The assignments of Rydberg states (Table IV) are made on the basis of the solution to Eq. (1), either in groups of states, or singly. The calculated values are extracted from the full set of calculated values given in the supplementary material,[45] and are based on the process identified in the experimental analysis. Thus, the calculated energies are all diagonalized results of the MRD-CI process. More details of the subset of calculated Rydberg states are given in Table II. Least squares fit between the observed Rydberg state energies in column 1 (x) and the calculated ones in column 6 (y) with form: y = A + Bx has A = −0.54(48) and B = 1.06(6), where the standard deviations for the last digit are given. The median and maximum absolute errors are 0.26 and 0.52 eV. The

correlation line effectively goes through the origin, has acceptable slope, but significant errors for several states in Table IV (for example, $3b_1$4D and $8b_2$4P).

VI. INTERPRETATION OF THE UV+VUV PHOTOABSORPTION SPECTRUM

A. The experimental envelope between 3.8 and 5 eV

The original onset assignment was as an $n\pi^*$ excitation;[12] however, Bist *et al.*,[16,17] who identified all the fundamental modes, showed that the rotational band structure was only compatible with a $\pi\pi^*$ ($^1B_2$) transition, which was confirmed by Nakagawa *et al.*[13] from jet cooled spectra. Our spectrum (Fig. 4) shows the main features seen in the previous high-resolution study. Our lowest calculated singlet state energies for 1^1B_2 ($3b_12a_2^*$, $\pi\pi^*$) are close to the experimental UV onset of 3.64 eV;[30,32] the MCSCF values are 3.65 eV, while UB3LYP yields 3.58 eV. Our calculated excitation vibrational frequencies for this 1^1B_2 state are close to those measured by Bist *et al.*;[16,17] a linear correlation of form: $Y_{Calc} = A + BX_{Observed}$ between the theoretical (Y, un-scaled harmonic) and observed (X) sets for all 30 vibration frequencies, shows that our calculated values are high by about 7%. The 1^1B_2 state structure determined by the MCSCF method, together with the excited state vibrational correlation with the experimental interpretation is shown in the supplementary material.[45]

B. The experimental envelope between 5.4 and 6.5 eV

For this region of the VUV spectrum, to make comparison with previous work[18] more directly, we give band positions in both cm^{-1} and eV. The first multiplet is part of a more intense complex band (Fig. 6) with origin at 5.62 eV (45 350 cm^{-1}) also observed by Berezin *et al.*[18] The envelope maximum is at 5.71 eV (46 060 cm^{-1}). We believe there are two very weak $^1B_1$ valence states here, together with the underlying $3b_1$3S state slightly higher in energy. To reduce the dynamic range of the spectrum, a broad Gaussian peak has been subtracted from Fig. 6. The IE_2 ($8b_2$ vacated) UPS envelope cannot be successfully overlaid here, and this result leads to assignment as a valence state.

The closely placed doublet at 6.28 eV (Fig. 7) is confirmed by overlay of the UPS and VUV spectra as a pair of 3*p*-Rydberg states ($\delta = 0.457$); the calculations suggest, on intensity grounds, that these are probably $^1B_2$ (3Y) and $^1B_1$ (3X) states. Even after ignoring the pair of (optically forbidden) 1^1A_2 states ($1a_217a_1^*$, and $3b_19b_2^*$), the region from 5.5 to 6.1 eV remains a complex part of the absorption spectrum.

C. The experimental envelope between 6.5 and 7.3 eV

Several examples of close identity of the UPS band 1 envelope with portions of the VUV spectrum occur above 6.7 eV. Figure 8 shows a pair of 3*d*-Rydberg states, identified from the much lower quantum defect, δ 0.091(at 6.79 eV) and 0.030 (at 6.85 eV) (the red and blue curves). However, even this seems an incomplete analysis, since double subtraction of these peaks using the IE_1 ($^2B_1$) ionic state envelope, does not account in full for the VUV spectral profile in this energy range. The twin peaks at 6.85 and 6.99 eV are slightly different in shape with wider vibration frequency from those relating to IE_1, and can be identified with the IE_2 ($^2B_2$) ionic state (Fig. 5). Thus, the region between 6.8 and 7.3 eV shows three Rydberg states, where two relate to IE_1 and one to IE_2.

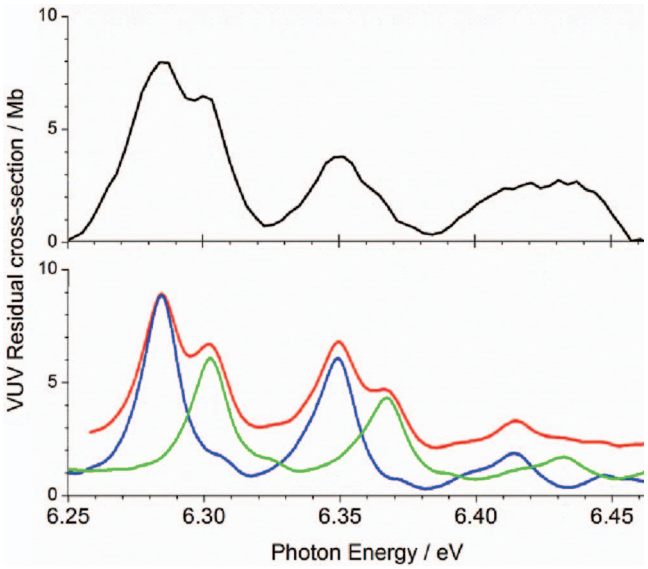

FIG. 7. VUV spectral structure near 6.3 eV (top curve in black) after subtraction of a broad Gaussian peak, and (bottom) the 7.310 eV Rydberg state structure positioned to simulate the main peak with its shoulder at 6.284(2) and 6.302(2) eV, showing the presence of a pair of $3b_1$3P Rydberg states based on IE_1.

D. The experimental envelope between 7.3 and 9.2 eV

The most detailed assignments occur in this region. Figure 9 shows three IE_1 excitations to higher principal quantum number (n) in the region 7.3–7.8 eV. The region between 8.1 and 9.2 eV is almost completely assigned (Fig. 10 shows part of this congested region) with excitations involving IE_2 ($^2B_2$), and IE_3 ($^2A_2$). The profile of

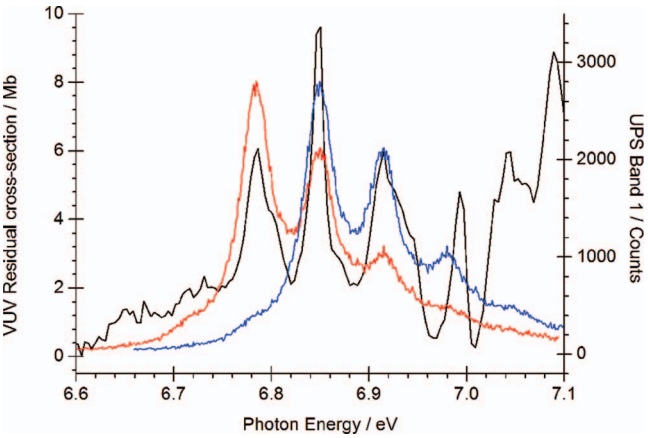

FIG. 8. Superposition of the UPS and VUV spectral envelopes near 6.8 eV showing the presence of two $3b_1$3D Rydberg states based on IE_1. The baselines of the UPS and VUV have been made parallel by subtraction of a broad Gaussian peak from the VUV spectrum.

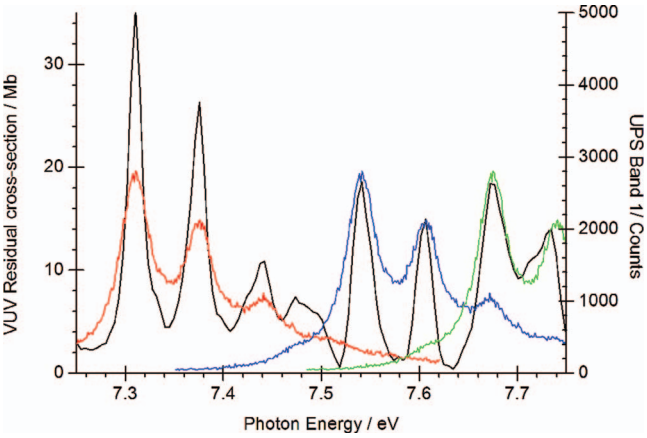

FIG. 9. The 7.2 to 7.7 eV region of the VUV spectrum, showing a variety of Rydberg state assignments; the UPS IE_1 ($^2B_1$) is shifted by 1.08 (red), 0.85 (blue), and 0.71 eV (green). The baselines of the UPS and VUV have been made parallel by subtraction of a broad Gaussian peak from the VUV spectrum.

IE_2 occurs in two areas that are free of other processes at 8.12 and 8.13 eV. The $1a_2nS$ series are forbidden, but the assignment shown for $n = 3$ is a $3p$-state with a comparatively high δ value (0.670). Above 9 eV (Table IV), the spectrum shows insufficient intensity for more than a few tentative assignments. A Rydberg state related to IE_4 is tentatively proposed at 10.04 eV ($2b_14S$), but this requires further positive identification. A much more highly resolved UPS as well as VUV spectrum is necessary to assist Rydberg state identification in this region.

VII. DISCUSSION AND CONCLUSIONS

The pyridine-N-oxide molecule is fairly rigid. The absence of negative vibration frequencies for a series of planar singlet excited and some ionized states shows the equilibrium structures are not saddle points which would show evidence of out-of-plane twisting. The principal bond variation in these higher states is the N–O bond.

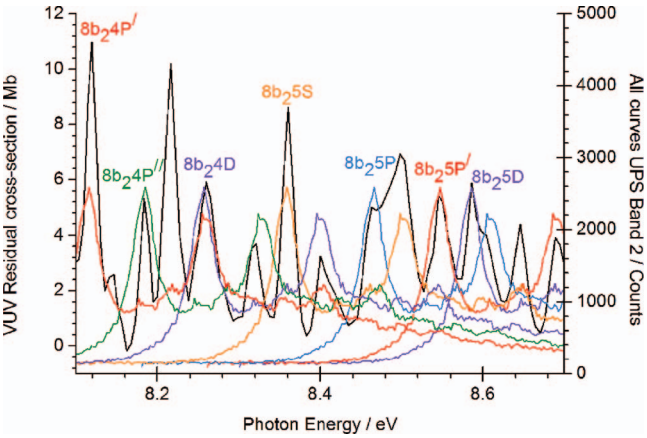

FIG. 10. The 8.1 to 8.7 eV region of the VUV spectrum (black), showing a variety of Rydberg state assignments (red, blue, and green) mostly based on IE_2 ($^2B_2$) excitations. The baselines of the UPS and VUV have been made parallel by subtraction of a broad Gaussian peak from the VUV spectrum.

The present valence state calculations at the MRD-CI highly correlated level for vertical excitation, and in parallel, MCSCF study of the adiabatic excitation energies both show a considerable number of valence states at low excitation energy. The prominence of these is probably a result of the highly polar nature of the **PyNO** molecule. Further, several of the valence states have high spectral intensity, and it appears that several Rydberg states fortuitously are superimposed on their broad (probably unresolved) maxima. Our calculated frequencies (Sec. VI A) for the onset $^1B_2$ state ($3b_12a_2^*$) correlate reasonably well with the experimental frequencies, with only two of the observed values determined from the spectral analysis by Bist *et al.*[16,17] significantly different.

For a molecule with 12 atoms, the VUV spectrum of **PyNO** is unexpectedly rich in Rydberg states. The present study identified several groups and individual states, with energies relating to the first three low-lying UPS bands. The first three IE states have the sequence $1^2B_1 < 1^2B_2 < 1^2A_2$; the Rydberg state energies, and separations of Rydberg states where a common upper level occurs (e.g., 3S or 3X etc.) also supports this sequence.

The UV+VUV spectrum of **PyNO** contains an extensive weak fine structure superimposed on broad high cross-section bands. A key feature of the present study was the identification of numerous Rydberg states of **PyNO** with limiting sequence energies at the first three low-lying UPS bands, and tentative suggestions for another converging on the fourth UPS band.

The superposition of the UPS and VUV spectra for **PyNO** allowed the identification of many Rydberg states in the VUV spectrum. Although the lowest Rydberg state ($3b_13S$) presented a challenge, we believe it is both very weak, but positively identified. By far the most heavily interpreted region of the VUV spectrum lies between 8.1 and 9.1 eV, where 12 Rydberg states were identified. The observation of so many of these Rydberg states lying above the first ionization limit, as super-excited states, is interesting. A feature of the UPS spectra is the relatively well-resolved vibrational structure of IE_1 through to IE_3; this implies that these vibrational states of the ions are relatively stable, and this in turn leads to significant sharpening of the Rydberg state profiles.

The lowest main UV band consists of a sharp valence state, but the present calculations suggest that the first main band centered on 4.4 eV is probably four valence states. Several other valence states were calculated to have high intensities, and it is suspected that these are responsible for much of the high cross-section absorption in the range 6–10.5 eV, since the Rydberg states have a very low intensity in all cases studied theoretically. There are few predicted examples of valence-Rydberg state mixing in this study.

ACKNOWLEDGMENTS

M.H.P. thanks the EPSRC UK National Service for Computational Chemistry Software (NSCCS) for computing support and Dr. P. Sherwood (Daresbury Laboratory) for maintenance of the GAMESS-UK suite of programmes. We thank

Dr. P. Kirsop for synthesis of the PyNO sample. D.L.L. thanks the National Science Foundation through Project Nos. CHE-0749530 and CHE-1111570, and the Department of Chemistry and Biochemistry, The University of Arizona, for support of the Molecular Photoelectron Spectroscopy facility. We thank a reviewer for helpful comments in relation to the nature of the orbitals in Fig. 2 and to the stability of vibrational states in the UPS spectrum.

[1]E. Ochiai, *Aromatic Amine Oxide* (Elsevier, Amsterdam 1967), p. 78.
[2]E. Ochiai, J. Org. Chem. **18**, 534 (1953).
[3]H. J. den Hertog and W. P. Combe, Recl. Trav. Chim. Pays-Bas Belg. **70**, 581–590 (1951).
[4]H. H. Jaffe, J. Am. Chem. Soc. **76**, 3527 (1954).
[5]R. D. Brown, F. R. Burden, and W. Garland, Chem. Phys. Lett. **7**, 461–462 (1970).
[6]O. Snerling, C. J. Nielsen, L. Nygaard, E. J. Pedersen, and G. O. Sørensen, J. Mol. Struct. **27**, 205–211 (1975).
[7]G. O. Sørensen, A. Tang-Pedersen, and E. J. Pedersen, J. Mol. Struct. **101**, 263–268 (1983).
[8]N. Heineking, H. Dreizler, K. Endo, and Y. Kamura, Z. Naturforsch., A: Phys. Sci. **44**, 1196–1200 (1989).
[9]J. F. Chiang, J. Chem. Phys. **61**, 1280–1283 (1974).
[10]D. Ülkü, B. P. Huddle, and J. C. Morrow, Acta Crystallogr. **27B**, 432–436 (1971).
[11]R. A. Aitken, B. Fodi, M. H. Palmer, A. M. Z. Slawina, and J. Yang, Tetrahedron **68**, 5845–5851 (2012).
[12]M. Ito and W. Mizushima, J. Chem. Phys. **24**, 495–500 (1956).
[13]Y. Nakagawa, I. Suzuka, and M. Ito, Chem. Phys. Lett. **208**, 453–459 (1993).
[14]J. C. D. Brand and K.-T. Tang, J. Mol. Spectrosc. **39**, 171–174 (1971).
[15]R. M. Hochstrasser and D. A. Wiersma, J. Chem. Phys. **55**, 5339–5343 (1971).
[16]H. D. Bist, J. S. Parihar, and J. C. D. Brand, J. Mol. Spectrosc. **59**, 435–441 (1976).
[17]H. D. Bist, J. S. Parihar, and J. C. D. Brand, J. Mol. Spectrosc. **64**, 211–216 (1977).
[18]K. V. Berezin, L. M. Babkov, and V. M. Bulanov, J. Struct. Chem. **36**, 309–313 (1995) [Zhur. Strukt. Khimii. **36**, 345 (1995)].
[19]J. P. Maier and J. F. Muller, J. Chem. Soc., Faraday Trans. 2 **70**, 1991–2003 (1974).
[20]L. Klasinc, I. Novak, G. Kluge, and M. Scholz, Z. Naturforsch. A **35A**, 656–8 (1980).
[21]G. Herzberg *Molecular Spectra and Molecular Structure. 3: Electronic Spectra and Electronic Structure of Polyatomic Molecules* (Krieger Publishing Company, Malabar, FL, 1991) (Reprinted).
[22]M. B. Robin, *Higher Excited States of Polyatomic Molecules* (Academic Press Inc., New York, 1974/1975/1985), Vols. 1–3 .
[23]M. S. Child, *Theory of Molecular Rydberg States, Cambridge Molecular Science* (Cambridge University Press, 2011).
[24]See Figure 1.2 in D. W. Turner, *Molecular Photoelectron Spectroscopy* (John Wiley & Sons Ltd., 1970), p. 5.
[25]I. C. Walker, M. H. Palmer, and A. Hopkirk, Chem. Phys. **141**, 365 (1989).
[26]R. Locht, B. Leyh, D. Dehareng, H. W. Jochims, and H. Baumgärtel, Chem. Phys. **362**, 97–108 (2009).
[27]P. Limão-Vieira, A. Giuliani, J. Delwiche, R. Parafita, R. Mota, D. Duflot, J. P. Flament, E. Drage, P. Cahillane, N. J. Mason, S. V. Hoffmann, and M.-J. Hubin-Franskin, Chem. Phys. **324**, 339–349 (2006).
[28]M. H. Palmer, S. V. Hoffmann, N. C. Jones, A. Head, and D. Lichtenberger, J. Chem. Phys. **134**, 084309 (2011).
[29]M. H. Palmer, P. J. Camp, S. V. Hoffmann, N. C. Jones, A. R. Head, and D. L. Lichtenberger, J. Chem. Phys. **136**, 094310 (2012).
[30]C. F. Dion and E. R. Bernstein, J. Chem. Phys. **103**, 4907 (1995).
[31]J. G. Philis, T. Mondal, and S. Mahapatra, Chem. Phys. Lett. **495**, 187 (2010).
[32]D. M. P. Holland, D. A. Shaw, M. Stener, and P. Decleva, J. Phys. B **42**, 245201 (2009).
[33]J. Pitarch-Ruiz, A. Sánchez de Merás, J. Sánchez-Marín, A. M. Velasco, C. Lavín, and I. Martín, J. Phys. Chem. A **112**, 3275 (2008).
[34]D. E. Love and K. D. Jordan, J. Phys. Chem. A **103**, 5667 (1999).
[35]H. Lefebvre-Brion, H. P. Liebermann, and G. J. Vazquez, J. Chem. Phys. **134**, 204104 (2011).
[36]M. P. Minitti, J. D. Cardoza, and P. M. Weber, J. Phys. Chem. A **110**, 10212 (2006).
[37]D. P. Seccombe, R. P. Tuckett, H. Baumgärtel, and H. W. Jochims, Phys. Chem. Chem. Phys. **1**, 773 (1999).
[38]R. J. Buenker, G. Hirsch and Y. Li, in *The Role of Rydberg States in Spectroscopy and Reactivity*, edited by C. Sandorfy (Kluwer, Dordrecht, 1999), pp. 57–91.
[39]H. Meyer, J. Chem. Phys. **107**, 7732 (1997).
[40]I. Ciofini and C. Adamo, J. Phys. Chem. A **111**, 5549 (2007).
[41]A. M. Velasco, J. Pitarch-Ruiz, A. M. J. Sánchez de Merás, J. Sánchez-Marin, and I. Martin, J. Chem. Phys. **124**, 124313 (2006).
[42]M. Warken, J. Chem. Phys. **103**, 5554 (1995).
[43]V. A. Shubert, M. Rednic, and S. T. Pratt, J. Chem. Phys. **132**, 124108 (2010).
[44]R. Mota, R. Parafita, A. Giuliani, M.-J. Hubin-Franskin, J. M. C. Lourenco, G. Garcia, S. V. Hoffmann, N. J. Mason, P. A. Ribeiro, M. Raposo, and P. Limão-Vieira, Chem. Phys. Lett. **416**, 152–159 (2005).
[45]See supplementary material at http://dx.doi.org/10.1063/1.4807841 for additional material relating to (a) the sample characterization and the spectroscopic methods; (b) the computational techniques for finding minimum energy structures and the planar cationic and singlet state structures of PyNO; (c) additional theoretical interpretation of the UPS spectrum; and (d) additional Figures showing specific spectral regions together with Rydberg states.
[46]M. F. Guest, I. J. Bush, H. J. J. Van Dam, P. Sherwood, J. M. H. Thomas, J. H. Van Lenthe, R. W. A. Havenith, and J. Kendrick, Mol. Phys. **103**, 719 (2005).
[47]H.-J. Werner, P. J. Knowles, F. R. Manby, M. Schütz *et al.*, MOLPRO, version 2010.1, a package of *ab initio* programs, 2010, see http://www.molpro.net.
[48]T. H. Dunning, J. Chem. Phys. **90**, 1007 (1989).
[49]R. J. Buenker and R. A. Phillips, J. Mol. Struct.: THEOCHEM **123**, 291 (1985).
[50]R. J. Buenker, in *Current Aspects of Quantum Chemistry*, edited by R. Carbó (Elsevier, New York, 1982), Vol. 21, pp. 17–21.
[51]R. J. Buenker and S. Krebs, "The configuration-driven approach for multireference configuration interaction calculations," in *Recent Advances in Multireference Methods*, edited by K. Hirao (World Scientific, Singapore, 1999), pp. 1–29.
[52]R. A. Kendall, T. H. Dunning, and R. J. Harrison, J. Chem. Phys. **96**, 6796 (1992).
[53]R. Ahlrichs and P. R. Taylor, J. Chim. Phys. Phys.-Chim. Biol. **78**, 315 (1981).
[54]M. H. Palmer, G. Ganzenmuller, and I. C. Walker, Chem. Phys. **334**, 154–166 (2007).
[55]J. Yang, J. Li, and Y. Mo, J. Chem. Phys. **125**, 174313 (2006).
[56]G. R. Cook and M. Ogawa, Can. J. Phys. **43**, 256–67 (1965).